

# Rényi entanglement entropies of descendant states in critical systems with boundaries: conformal field theory and spin chains

**Luca Taddia**

Scuola Normale Superiore, Piazza dei Cavalieri 7, I-56126 Pisa, Italy  
CNR - Istituto Nazionale di Ottica, Sede Secondaria di Sesto Fiorentino, Via Carrara 1, I-50019 Sesto Fiorentino, Italy  
E-mail: luca.taddia2@gmail.com

**Fabio Ortolani**

Dipartimento di Fisica e Astronomia dell'Università di Bologna & INFN, Sezione di Bologna, Via Imerio 46, I-40127 Bologna, Italy

**Tamás Pálmai**

MTA-BME “Lendulet” Statistical Field Theory Research Group, Institute of Physics, Budapest University of Technology and Economics, Budafoki ut 8, H-1111 Budapest, Hungary

**Abstract.** We discuss the Rényi entanglement entropies of descendant states in critical one-dimensional systems with boundaries, that map to boundary conformal field theories in the scaling limit. We unify the previous conformal-field-theory approaches to describe primary and descendant states in systems with both open and closed boundaries. We provide universal expressions for the first two descendants in the identity family. We apply our technique to critical systems belonging to different universality classes with non-trivial boundary conditions that preserve conformal invariance, and find excellent agreement with numerical results obtained for finite spin chains. We also demonstrate that entanglement entropies are a powerful tool to resolve degeneracy of higher excited states in critical lattice models.

## 1. Introduction

Understanding quantum correlations and entanglement in many-body systems is one of the main purposes of fundamental physics [1]. Although a general strategy for this task currently lacks, in the last decades many advances have been made. In particular, one-dimensional (1D) systems play a very special role in this scenario, for two reasons: the first is of physical nature, and resides in the enhancement of the importance of quantum fluctuations, due to dimensionality [2]; the second is the existence of extremely powerful analytical and numerical techniques, such as exact solutions [3], bosonization [2], Bethe ansatz [4], and matrix-product-states algorithms [5], allowing for the extraction of accurate information about low-lying excitations in a non-perturbative way. Within the bosonization framework, the strategy is to identify the relevant degrees of freedom of the considered 1D model and, starting from them, to build up an effective field theory capturing

its low-energy physics [2]. If the ground state (GS) of the original model is gapless, the obtained field theory is usually conformally invariant, and is therefore called conformal field theory (CFT) [6, 7] (we remark that bosonization is not the only approach leading to effective CFT's; see, e.g., Ref. [8]). Due to their solvability in  $(1+1)\text{D}$ , CFT's are particularly useful, allowing for the exact computation of all correlation functions, and therefore providing access to many interesting quantities in a controllable way [9].

In the present work we deal with a particular class of entanglement measures, the Rényi entanglement entropies (REE's) [10, 11], defined in the following way. Let us consider a pure state of an extended quantum system, associated with a density matrix  $\hat{\rho}$ , and a spatial bipartition of the system itself, say  $\{A, B\}$ . If we are interested in computing quantities that are spatially restricted to  $A$ , we can employ, instead of the full density matrix, the reduced density matrix  $\hat{\rho}_A = \text{Tr}_B \hat{\rho}$ . The  $n$ -th REE, defined as

$$S_n(A) = \frac{1}{1-n} \log_2 \text{Tr}_A \hat{\rho}_A^n, \quad (1)$$

describes the reduced density matrix. In the limit  $n \rightarrow 1$  it reproduces the von Neumann entanglement entropy (VNEE)  $S(A) = -\text{Tr}_A [\hat{\rho}_A \log_2 \hat{\rho}_A]$ , the most common entanglement measure [11]. In the last decade, the  $n \neq 1$  REE's have also become quite popular, for several reasons. Analytical methods proved to be more suitable to calculate REE's than VNEE, especially in field theory: e.g., in CFT, REE's have a clear interpretation as partition functions, while the VNEE does not [12, 13]. From a fundamental point of view, the knowledge of the REE's  $\forall n \in \mathbb{N}$  is equivalent to the knowledge of  $\hat{\rho}_A$  itself, since they are proportional to the momenta of  $\hat{\rho}_A$ . At the same time, from a physical point of view, many of the important properties of the VNEE, e.g., the area law for gapped states [14, 15, 16] and the proportionality to the central charge for critical systems [17, 12, 13], carry over to REE's as well. In fact, REE's are easily computable by matrix-product-states algorithms [5], and they allow for a precise estimation of the central charge from numerical data regarding the GS of the system (see, e.g., Ref. [18]). Finally, and very importantly, measurements of the  $n = 2$  REE in an ultracold-atoms setup have been recently performed [19, 20], paving the way to the experimental study of entanglement measures in many-body systems.

The computations of Refs. [12, 13], that deal with the GS of CFT's, have been extended, in more recent times, to excited states [21, 22, 23, 24]. In CFT, excitations are in one-to-one correspondence with fields, and can be organized in conformal towers [7]. The lowest-energy state of each tower is in correspondence with a so-called *primary* field, while the remaining ones, called *descendant*, are in correspondence with *secondary* fields, obtained from the primaries by the application of conformal generators. While the properties of REE's for primary states are now quite well understood [21, 22, 23], much less is known about the descendants. In the pioneering work of Ref. [24], a unifying picture for the computation of REE's of primary and descendant states was developed and both analytical and numerical computations for the scaling limit of simple spin chains with periodic boundary conditions (PBC) were performed. A related but physically different problem was considered in Refs. [25, 26], where the effect on the time evolution of inserting secondary operators at finite time was studied.

In this paper we continue the work in Ref. [24] and extend its framework to the case of open boundary conditions (OBC) that preserve conformal invariance. This is an important step, for several reasons. First, impurity problems [27] and certain problems in string theory [28] map to boundary CFT; not secondarily, the experimentally achievable setups often involve OBC. The importance of descendant states stems from novel applications, including non-trivial checks of the universality class of critical lattice models, and understanding the behavior of degenerate multiplets.

We will provide a general strategy for the computation of REE's, derive CFT predictions for descendant states, and compare them to the numerical data obtained from lattice realizations of the considered CFT's. We will also discuss some interesting complementary aspects arising naturally when considering descendant states: e.g., we will need to consider the REE's of linear combinations on the CFT side, in order to study degenerate states in the XX chain.

The paper is structured as follows. In Section 2 we will review the approach of Ref. [24] for systems with PBC, derive the procedure to compute the REE's for descendant states in CFT's with (and without) boundaries, and provide some general results for states related to the tower of the identity. In Section 3 we will compute explicitly the REE's for the  $c = 1/2$  minimal CFT, and compare the scalings to the numerical data obtained for the spin-1/2 Ising model in a transverse field; in Section 4 we will perform the same study for the  $c = 4/5$  minimal CFT and the three-state Potts model, while in Section 5 for the compactified free boson and the spin-1/2 XX chain. In Section 6 we will draw our conclusions and some directions for future work. In the Appendixes we will provide useful technical details of our discussion.

## 2. Results from CFT

In the scaling limit, critical 1D lattice models can be described by CFT's [2, 8]. Since CFT's are exactly solvable, explicit universal expressions can be derived for the REE's. In this Section we describe a calculation scheme for the REE's of arbitrary excited states in CFT unifying the cases of PBC and OBC. We consider here only unitary theories; see Ref. [29] for a generalization to the ground states of non-unitary models.

### 2.1. Periodic boundary conditions

The case of a finite system with PBC has been widely studied in the past (see, e.g., Refs. [12, 13, 21, 22, 24]). In this Section, we review the computation of the REE's for excited states in this case, following the approach of Refs. [22, 24] and modifying it slightly, having in mind the generalization to the OBC case.

We consider an Euclidean space-time manifold of an infinite cylinder: it is characterized by the complex variable  $r - i\tau$ , being  $r$  a space coordinate, and  $\tau$  a time one;  $r - i\tau$  and  $r + L - i\tau$ , where  $L$  is the size of the system (acting as an IR cutoff for the field theory), are identified. The physical support is the circle at  $\tau = 0$ ; the subsystem  $A$  is chosen to be the interval  $[-\ell/2, \ell/2]$ . The zero-temperature density matrix of the system is pure, i.e.,  $\hat{\rho}_\Psi = |\Psi\rangle\langle\Psi|$ , where  $|\Psi\rangle$  is a generic eigenstate of the Hamiltonian.

The starting point of our computation is the following identity:

$$\mathrm{Tr}_A \rho_{A,\Psi}^n = \sum_{a_1 b_1} \sum_{a_2 b_2} \dots \sum_{a_n b_n} \langle a_1 b_1 | \Psi \rangle \langle \Psi | a_2 b_1 \rangle \langle a_2 b_2 | \Psi \rangle \langle \Psi | a_3 b_2 \rangle \dots \langle a_n b_n | \Psi \rangle \langle \Psi | a_1 b_n \rangle, \quad (2)$$

where we repeatedly inserted resolutions of the identity for the Hilbert spaces relative to the segments  $A$  and  $B$ . Because of the state-operator correspondence in CFT, each eigenstate is generated by an operator  $\Psi$ , acting on the vacuum and placed at the infinite past [7]. Adopting this representation, the overlaps above are nothing but path integrals on half of the infinite complex cylinder, with the insertions of  $\Psi$  and  $\Psi^\dagger$  in the far past and future respectively, and with boundary states  $a_i$  and  $b_j$  along the segments  $A$  and  $B$ . When the sums in Eq. (2) are performed we obtain a correlation function of  $\Psi$  and  $\Psi^\dagger$  operators on the so-called *replica manifold*, consisting of  $n$  copies of the cylinder, glued together cyclically across cuts along  $A$  [12, 13]. Each of the  $n$

copies can be transformed to the complex plane by the conformal mapping  $\xi_j = e^{i\frac{2\pi}{L}(r_j - i\tau_j)}$  [7]: the resulting  $n$ -sheeted manifold, that will be denoted by  $\mathcal{R}_n$ , is a collection of  $n$  planes glued across the boundaries  $(\mathcal{A} \pm a)_j$  according to  $(\mathcal{A} - a)_j \leftrightarrow (\mathcal{A} + a)_{j+1}$ , where  $\mathcal{A}$  is the arc of the unit circle  $e^{i\phi}$ ,  $\phi \in [-\pi x, \pi x]$  ( $x = \ell/L$  is the relative subsystem size), and  $a$  is a radial infinitesimal vector (related to, e.g., the lattice spacing in the case of a lattice model), introduced in order to UV-regularize the theory.

Assuming the usual normalization for the state, i.e.,  $\langle \Psi | \Psi \rangle_{\mathcal{R}_1} = 1$ ,  $\text{Tr}_A \rho_{A, \Psi}^n$  reduces to a  $2n$ -point function on the replica manifold, that we then transform into a  $2n$ -point function on a single plane (the following relation contains a non-trivial statement: see the end of this Section for a clarification of this point):

$$\text{Tr}_A \rho_{A, \Psi}^n = \mathcal{N}_n \left\langle \prod_{j=1}^n \Psi(0_j, 0_j) \Psi(0_j, 0_j)^\dagger \right\rangle_{\mathcal{R}_n} = \mathcal{N}_n \left\langle \prod_{j=1}^n \mathcal{T}_{f_{n,x}} \Psi(0_j, 0_j) \mathcal{T}_{f_{n,x}} \Psi(0_j, 0_j)^\dagger \right\rangle_{\mathbb{C}}, \quad (3)$$

where the constant  $\mathcal{N}_n = Z_n/Z_1^n$  ( $Z_n$  is the partition function over  $\mathcal{R}_n$ ) sets the correct normalization  $\text{Tr}_A \rho_{A, \Psi} = 1$ , and takes, in the present case, the form

$$\mathcal{N}_n = \left[ \frac{L}{\pi a} \sin(\pi x) \right]^{\frac{c}{6} \left( \frac{1}{n} - n \right)}, \quad (4)$$

where  $c$  is the central charge of the considered CFT [7]. The second expression in Eq. (3) is obtained by means of the conformal mapping  $\xi \rightarrow f_{n,x}(\xi)$  from  $\mathcal{R}_n$  to the complex plane, i.e., a composition of a Möbius transformation and the  $n$ -th root:

$$f_{n,x}(\xi) = \left( \frac{e^{-i\pi x} \xi - 1}{\xi - e^{-i\pi x}} \right)^{1/n}. \quad (5)$$

The Möbius transformation brings the cut along the arc  $\mathcal{A}$  to the half line  $(-\infty, 0]$ ; then, the  $n$ -th root transforms each replica sheet to a slice of the complex plane. We prescribe the  $j$ -th sheet ( $j = 1, \dots, n$ ) to be transformed by the  $j$ -th branch of the  $n$ -th root. The mapping for  $n = 2$  is represented graphically in Figure 1. Finally, the operator  $\Psi(z)$  is transformed into  $\mathcal{T}_{f_{n,x}} \Psi(z)$  under the mapping (5). The symbol  $\mathcal{T}$  is not to be confused with the twist operator appearing when the Rényi entropy is expressed as a quantity in a local theory [30]. The transformed operator is inserted at the point  $f_{n,x}(z)$ ; for details see Appendix A.

The normalization constant can be identified (apart from a non-universal additive constant; see Eq. (11)) with the GS contribution

$$S_n^{\text{GS}} = \frac{1}{1-n} \log_2 \mathcal{N}_n; \quad (6)$$

then if we rewrite the REE as

$$S_n^\Psi = S_n^{\text{GS}} + \frac{1}{1-n} \log_2 F_\Psi^{(n)}, \quad (7)$$

the  $n$ -th (exponentiated) *excess entanglement entropy* (EEE)  $F_\Psi^{(n)}$  corresponds to the  $2n$ -point function

$$F_\Psi^{(n)} = \left\langle \prod_{j=1}^n \mathcal{T}_{f_{n,x}} \Psi(0_j, 0_j) \mathcal{T}_{f_{n,x}} \Psi(0_j, 0_j)^\dagger \right\rangle_{\mathbb{C}}. \quad (8)$$

Interestingly, from the CFT point of view,  $F_\Psi^{(n)}$  is intrinsically regular, since the cutoffs  $a$  and  $L$  only appear in multiplicative state-independent factors in the normalization  $\mathcal{N}_n$ .

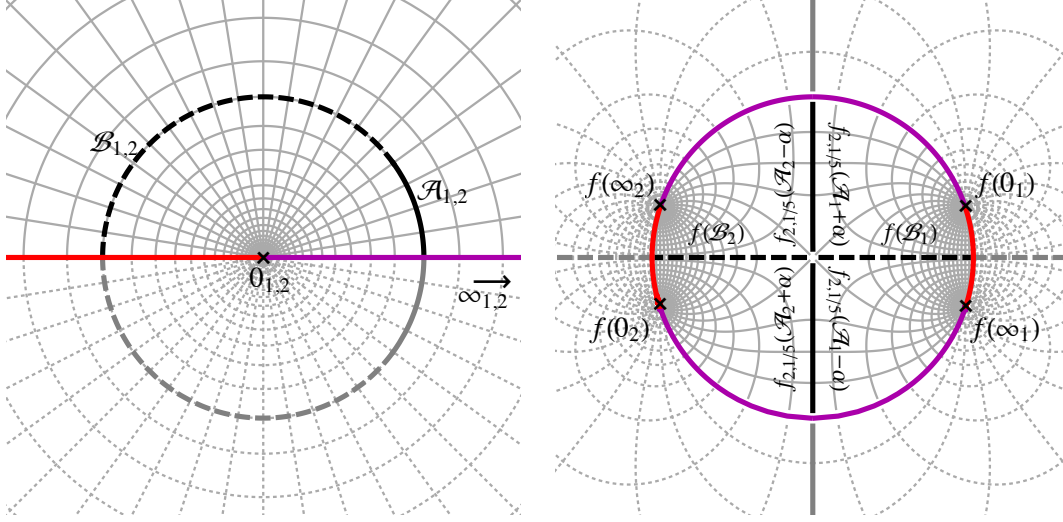


**Figure 1.** Conformal map  $f_{2,1/5}$  regularizing the replica manifold for both PBC and OBC. The mesh represent lines of equal time and space coordinates. In the OBC case only the solid lines are in the physical domain. The purple (red) line represents the left (right) edge of the OBC strip. Left panel: pre-transformed space-time. Right panel: transformed space-time.

The EEE is related to the relative Rényi entropy of the excited state compared to the vacuum (for some recent general results on relative entropies in 2D CFT see Ref. [31]). The relative entropy is defined as

$$S_n(\rho_\Psi || \rho_\Phi) = \frac{1}{n-1} (\log_2 \text{Tr} \rho_\Psi^n - \log_2 \text{Tr} \rho_\Psi \rho_\Phi^{n-1}). \quad (9)$$

The  $n$ -th excess and relative entropies compared to the vacuum (i.e.  $\Phi = 1$ ) are related by the following:

$$S_n(\rho_\Psi || \rho_\Phi) = \frac{1}{n-1} \left( \log_2 F_\Psi^{(n)} - \log_2 \langle \mathcal{T}_{f_n, x} \Psi(0_1, 0_1) \mathcal{T}_{f_n, x} \Psi(0_1, 0_1)^\dagger \rangle_{\mathbb{C}} \right) \quad (10)$$

. The appearing two-point functions can be calculated straightforwardly once the transformation laws are known.

The best-known result that can be obtained from Eq. (3) is the following formula for the REE's of the GS of a finite system with PBC [12]. Such state is associated with the identity operator, for which the correlation function in Eq. (3) is 1 and only the constant  $\mathcal{N}_n$  plays a role. Explicitly, Eq. (6) looks:

$$S_n^{\text{GS}}(x, L) = \frac{c}{6} \left( 1 + \frac{1}{n} \right) \log_2 \left[ \frac{L}{\pi} \sin(\pi x) \right] + c_n, \quad (11)$$

where  $c_n$  is a non-universal constant accounting for regularization. This formula has become, in the years, the most used tool in order to extract the central charge of a CFT from finite-size numerical data: for most of the available algorithms, REE's are among the most natural quantities to compute [5, 32]. Moreover, traditional numerical methods need, in order to compute the central charge, the knowledge of information about both GS and the first excitations [33, 34], while Eq. (11) just involves data from the former.

If  $\Psi$  is not the identity, corrections can arise, their precise shape depending on the considered CFT and the operator itself. Such corrections can be computed using some results from meromorphic CFT [35]. First, the adjoint of a field can be obtained by transforming it according to the map  $z \rightarrow z^{-1}$  [7]; moreover, a sequence of mappings  $z \rightarrow f(z) \rightarrow g(f(z))$  has the same effect on any operator as the single transformation  $z \rightarrow g(f(z))$ , since only derivatives, logarithmic derivatives and derivatives of the Schwarzian derivative [7] occur in the transformation laws (see Appendix A). Therefore, using the relations

$$\mathcal{T}_{f_{n,x}}\Psi(0)^\dagger = \mathcal{T}_{g_{n,x}}\Psi(0), \quad g_{n,x}(\xi) = f_{n,x}(1/\xi) = f_{n,-x}(\xi), \quad (12)$$

(we supposed the field to be real), the  $n$ -th EEE reads

$$F_\Psi^{(n)} = \left\langle \prod_{j=1}^n \mathcal{T}_{f_{n,x}}\Psi(0_j, 0_j) \mathcal{T}_{f_{n,-x}}\Psi(0_j, 0_j) \right\rangle_{\mathbb{C}}. \quad (13)$$

The operators  $\mathcal{T}_{f_{n,x}}\Psi$  can be determined straightforwardly from  $\Psi$ . The generic transformation rule for secondary fields [36] yields a sum of lower descendants in the same tower (see Appendix A for details): the resulting  $2n$ -point functions of secondary fields are thus evaluated by relating them to  $2n$ -point functions of primaries. The two are in general connected by the action of a complicated differential operator, which however can be determined (case by case) by means of a systematic approach (see Ref. [24] and Appendix B). Following this program, the  $n$ -th EEE finally looks

$$F_\Psi^{(n)} = \mathcal{D}_{x,n}^\Psi \left\langle \prod_{j=1}^n \Xi(z_j^+, \bar{z}_j^+) \Xi(z_j^-, \bar{z}_j^-) \right\rangle, \quad z_j^\pm = e^{\frac{ix}{n}(\pm x + 2j - 2)}, \quad (14)$$

where  $\mathcal{D}_n^\Psi(x)$  is the cited differential operator, and  $\Xi$  is the primary field in the tower of  $\Psi$ . In this work, we will need the explicit form of a number of such  $2n$ -point functions of primary fields. In some cases, we will use, when available, known results from the literature; in the remaining ones, we will compute the correlations by means of the Coulomb-gas approach [7], or different representations of the considered CFT allowing for their derivation.

Finally, we remark that the strategy described in this Section and adopted in Ref. [24] is not exactly the one used in Ref. [22] for primary states of periodic systems. In particular, we treated the problem starting directly from a replica manifold of planes, instead of “physical” cylinders. Descendant states,  $\Psi(0)|0\rangle$ , are more naturally defined on the plane, where the physical Hamiltonian takes the form  $H \sim L_0 + \bar{L}_0$  and descendants are obtained by acting with strings of Virasoro generators on primary states [7]. Furthermore, we are allowed to start from planes since a sequence of two conformal mappings using two given holomorphic functions is equivalent to one map under the composition of these functions. Coming back to the physical manifold would be redundant, and more importantly, we observed that starting from the planes simplifies the actual computations substantially by removing uncomfortable infinities, that would need careful regularization. We will use this approach also for the case of OBC.

## 2.2. Open boundary conditions

In CFT, OBC reduce the operator content of the theory, and for minimal models the OBC preserving conformal invariance are in one-to-one correspondence with the primary fields of the theory on the plane [37]. The partition function of a CFT on the upper half plane, that is the prototypical boundary manifold, looks [7]

$$Z_{\alpha\beta}(q) = \sum_h \mathcal{N}_{\alpha\beta}^h \chi_h(q), \quad (15)$$

with  $\alpha$  and  $\beta$  being conformal weights of primary fields, indexing the possible conformal OBC,  $\mathcal{N}_{\alpha\beta}^h$  the fusion coefficients, and  $\chi_h(q)$  the character corresponding to the primary operator of chiral dimension  $h$ . By expanding Eq. (15) around  $q = 0$ , a series is obtained, whose integer coefficients are the degeneracies of the energy levels.

For OBC, the physical space-time is an infinite strip of finite width  $L$ , described, again, by the complex variable  $r - i\tau$ ; the subsystem  $A$  is taken as the  $\tau = 0$  interval  $[0, \ell]$ . The infinite strip can be mapped to the upper half plane by the transformation  $\xi = e^{i\frac{\pi}{L}(r-i\tau)}$  [7];  $A$  is then mapped to the unit arc  $\mathcal{A}$  connecting 0 and  $e^{i\pi x}$ , and the operators associated with the excitation are placed at the origin and at infinity.

Opportunistically, we set up our framework for the REE in the previous subsection in a way that it needs no modification for OBC. We use the same mapping (5) unifying in this case the  $n$  half-planes to a single unit disk (see Figure 1). After the transformation, the operators lie on the boundaries of the disk separating arcs with different conformal OBC. The resulting  $2n$ -point functions can be evaluated using boundary CFT: compared to the PBC case now one of the chiralities is suppressed and the chiral building blocks (conformal blocks) combine with different, boundary-dependent, coefficients. This can be understood considering that with OBC present in the system, some fusion channels, open in the PBC case, are now closed and the operator product expansion coefficients [38, 39] determining the weight of the conformal blocks in the  $2n$ -point functions change. In particular, in the fusion of the boundary operators  $\Phi_i^{(\alpha\beta)}(z_i)$  and  $\Phi_j^{(\beta\gamma)}(z_j)$ , changing the boundary condition at the insertion points from  $\alpha$  to  $\beta$  and  $\beta$  to  $\gamma$ , respectively, will only involve fields whose towers are present in the partition function  $Z_{\alpha\gamma}$  (see Eq. (15)). This fact will be very useful in the situations where we will have to decide which fusion channels are to be considered in order to compute the desired correlators.

### 2.3. The identity tower

We now discuss the EEE for states associated to fields in the tower of the identity. Such states are present in any bulk CFT, and are also very common for theories living on manifolds with boundaries. Moreover, they have the property of depending explicitly on the central charge of the CFT: they thus allow, in principle, the determination of  $c$  from numerical data, generalizing what is usually done for the GS to the whole tower.

As an example, we compute the  $n = 2$  EEE for the first descendant in the tower, i.e., the state associated with the stress-energy tensor  $T = L_{-2}\mathbb{I}$  ( $\{L_p, p \in \mathbb{Z}\}$  form the Virasoro algebra [7]). Its transformation under a conformal map  $f$  is

$$U_f^{-1}(L_{-2}\mathbb{I})(\xi)U_f = [f'(\xi)]^2(L_{-2}\mathbb{I})(f(\xi)) + \frac{c}{12}\{f, \xi\}\mathbb{I}, \quad (16)$$

being  $\{f, \xi\} = f'''(\xi)/f'(\xi) - 3[f''(\xi)/f'(\xi)]^2/2$  the Schwarzian derivative of  $f$ . We can thus write

$$\langle (L_{-2}\mathbb{I})(0_1)(L_{-2}\mathbb{I})(0_1)^\dagger(L_{-2}\mathbb{I})(0_2)(L_{-2}\mathbb{I})(0_2)^\dagger \rangle_{\mathcal{R}_2} = \sum_{j,k,l,m=1}^2 C_{1j}C_{2k}C_{3l}C_{4m}P_{jklm}, \quad (17)$$

where  $P_{jklm} = \langle \phi_j(z_1^+)\phi_k(z_1^-)\phi_l(z_2^+)\phi_m(z_2^-) \rangle$  is the collection of complex-plane four-point functions of the operators  $\phi_1 = \mathbb{I}$  and  $\phi_2 = L_{-2}\mathbb{I}$  inserted at the appropriate points; the matrix  $C$  contains the (potentially vanishing) coefficients of the different correlations, and it can be guessed from the

transformation relations

$$\begin{aligned}\mathcal{T}_{f_{2,x}}(L_{-2}\mathbb{I})(0_1) &= \sin^2(\pi x) \left[ \frac{c}{8} \mathbb{I} - e^{i\pi x} (L_{-2}\mathbb{I}) \right] \left( +e^{+i\pi x/2} \right), \\ \mathcal{T}_{f_{2,x}}(L_{-2}\mathbb{I})(0_2) &= \sin^2(\pi x) \left[ \frac{c}{8} \mathbb{I} - e^{i\pi x} (L_{-2}\mathbb{I}) \right] \left( -e^{+i\pi x/2} \right).\end{aligned}\tag{18}$$

To obtain  $P_{jklm}$ , we employ the recipe described in Appendix B and derive the two-, three- and four-point functions of the stress-energy tensor ( $T$  is self-adjoint):

$$\begin{aligned}\langle (L_{-2}\mathbb{I})(z_1) \rangle &= 0 \\ \langle (L_{-2}\mathbb{I})(z_1) (L_{-2}\mathbb{I})(z_2) \rangle &= \frac{c}{2z_{12}^4}, \\ \langle (L_{-2}\mathbb{I})(z_1) (L_{-2}\mathbb{I})(z_2) (L_{-2}\mathbb{I})(z_3) \rangle &= \frac{c}{z_{12}^2 z_{13}^2 z_{23}^2}, \\ \langle (L_{-2}\mathbb{I})(z_1) (L_{-2}\mathbb{I})(z_2) (L_{-2}\mathbb{I})(z_3) (L_{-2}\mathbb{I})(z_4) \rangle &= \sum_{jkl=234,324,423} \frac{c^2/4}{z_{1j}^4 z_{kl}^4} + \\ &\quad + 2c \frac{\sum_{j<k} z_j^2 z_k^2 - \sum_j \sum_{k<l \in \{1,2,3,4\} \setminus j} z_j^2 z_k z_l + 6z_1 z_2 z_3 z_4}{\sum_{j<k} z_{jk}^2}.\end{aligned}\tag{19}$$

being  $z_{jk} = z_j - z_k$ . After substituting  $z_{1,2}^\pm$ , performing the sums in Eq. (17) with the appropriate coefficients  $C$ , determined from (18), and multiplying by the normalization  $\sqrt{c/2}$  for the state  $|L_{-2}\mathbb{I}\rangle$ , we obtain

$$\begin{aligned}F_T^{(2)}(x) &= \frac{\sin^4(\pi x) [\cos(2\pi x) + 7]}{16} c^{-1} + \\ &\quad + \frac{16200 \cos(2\pi x) - 228 \cos(4\pi x) + 120 \cos(6\pi x) + \cos(8\pi x) + 16675}{32768} + \\ &\quad + \frac{\sin^4(\pi x) [\cos(2\pi x) + 7]^2}{1024} c + \frac{\sin^8(\pi x)}{1024} c^2,\end{aligned}\tag{20}$$

that is what we will compare to numerical data in the next Sections.

Before doing it, it is worth to analyze Eq. (20) both as a function of the relative subsystem size  $x$  and of the central charge  $c$ . In Fig. 2(a) we show  $F_T^{(2)}(x)$  for different values of  $c$ . We observe that the small-block EEE is independent of  $c$ , which can also be seen by expanding  $F_T^{(2)}(x)$  around  $x = 0$ :

$$F_T^{(2)}(x) = 1 - (\pi x)^2 + \frac{3c^2 + 22c + 24}{48c} (\pi x)^4 - \frac{105c^2 + 364c + 660}{1440c} (\pi x)^6 + O(x^8).\tag{21}$$

This behavior is in agreement with the holographic result of Ref. [42], where it was established that the excess VNEE is proportional to the excitation energy, i.e.,  $\Delta S = \frac{1}{3}\pi x \Delta E$ , and in particular it is independent of  $c$ . In the opposite limit, the half-block EEE is given by

$$F_T^{(2)}(1/2) = \frac{1}{256} \left( \frac{c^2}{4} + 9c + 1 + \frac{3}{32c} \right).\tag{22}$$

Interestingly, this function features a minimum located at  $c_{\min} \approx 3.02212$ . For small  $c$ , the whole function  $F_T^{(2)}(x)$  diverges, signaling that in a  $c = 0$  unitary CFT only the vacuum state exists [40]. When  $c$  is large, we see from the curves of Fig. 2(a) that the leading term  $c^2 \sin^8(\pi x)/1024$  starts to dominate. This leading term emerges when taking only the contributions of the identity in the



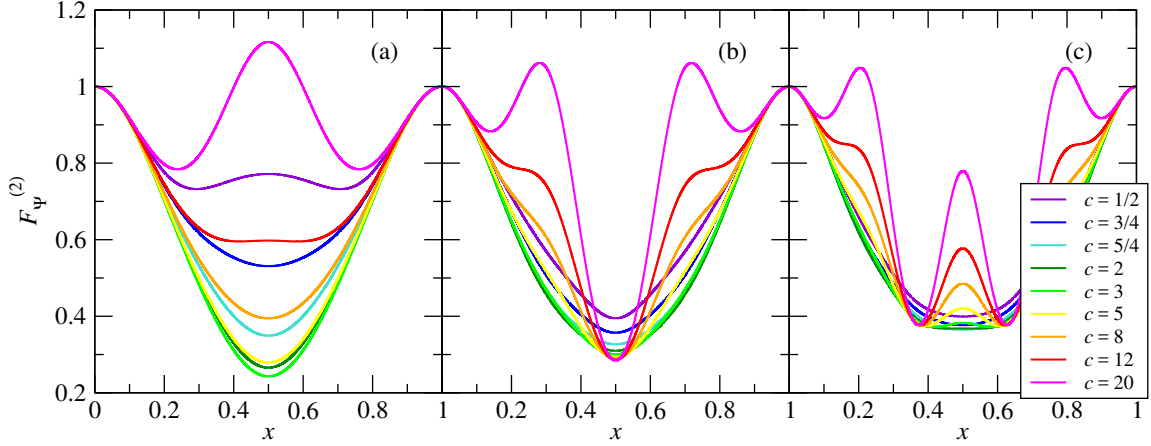


**Figure 2.**  $F_{\Psi}^{(2)}(x)$  for  $\Psi = L_{-2}$  (panel (a)),  $L_{-3}$  (panel (b)) and  $L_{-4}$  (panel (c)), for several values of the central charge  $c$ .

transformation laws (16). This is the regime where the AdS/CFT correspondence should play a role (see, for a review, e.g., Ref. [41]); however, to our knowledge, this result is not yet available in that context (again, we remark that results for the small-block limit are already available [42].)

While in the present work we will only use the result for the stress-energy tensor, we emphasize that by means of the general transformation rule described in Appendix A a similar analysis can be carried out for the whole identity tower. E.g., for the state related to  $L_{-3}\mathbb{I}$  we obtain

$$\begin{aligned}
F_{L_{-3}\mathbb{I}}^{(2)} = & \frac{\sin^4(\pi x) [8391 \cos(2\pi x) + 1890 \cos(4\pi x) + 361 \cos(6\pi x) + 7790]}{16384} c^{-1} + \\
& + \frac{3032808 \cos(2\pi x) + 819919 \cos(4\pi x) - 27612 \cos(6\pi x)}{8388608} + \\
& + \frac{386 \cos(8\pi x) + 8436 \cos(10\pi x) + 289 \cos(12\pi x) + 4554382}{8388608} + \\
& + \frac{\sin^4(\pi x) \cos^2(\pi x) [255 \cos(2\pi x) + 90 \cos(4\pi x) + 17 \cos(6\pi x) + 1686]}{8192} c \\
& + \frac{\sin^8(\pi x) \cos^4(\pi x)}{64} c^2.
\end{aligned} \tag{23}$$

In Figs. 2(b) and (c) we show the  $n = 2$  EEE's for  $L_{-3}|0\rangle$  and  $L_{-4}|0\rangle$  and several values of the central charge. Similarly to the case of  $L_{-2}|0\rangle$ , the higher descendants also show a  $c$ -independence for small blocks, in agreement with Ref. [42]. Comparing the three panels of Fig. 2, we observe that, increasing the level of the excitation, the shape of the curves for  $c \lesssim 3$  (these values of course include minimal models) becomes less and less dependent on the actual value of the central charge.

### 3. $c = 1/2$ minimal theory and spin-1/2 Ising chain in a transverse field

In this Section, we present analytical predictions for the  $c = 1/2$  minimal CFT, and numerical data relative to the  $n = 2$  REE for the descendant states of the spin-1/2 Ising chain in a transverse

field. The REE's for the primary states were already discussed in Ref. [23]; here, we just focus on descendant states.

The  $c = 1/2$  minimal model is one of the simplest CFT's [7]. The operator content of the model on the plane is the following: the primary fields are the identity and the fields  $\sigma$  and  $\psi$ , of chiral dimension 0,  $1/16$ , and  $1/2$ , respectively. For minimal models on the upper half plane, the BC preserving conformal invariance are in one-to-one correspondence with such primary fields, leading, as we shall see, to four possible pairs of OBC. In this Section we will consider, in any case, the first descendant state in each conformal tower.

A 1D lattice realization of the  $c = 1/2$  minimal CFT is the spin-1/2 Ising chain in a transverse field at the critical point [8]. The Hamiltonian of such chain is given by

$$H = -J \sum_j \sigma_j^z \sigma_{j+1}^z - h \sum_j \sigma_j^x, \quad (24)$$

where  $\sigma_j^\alpha$  is a Pauli matrix ( $\alpha = x, y, z$ ) at the site  $j \in \{1, 2, \dots, L\}$ ; the critical point is located at  $h/J = 1$ . The three possible conformal OBC are the following [43, 44]: the  $x$ -component of the boundary spins must be fixed to  $1/2$  (+),  $-1/2$  (-) or let free ( $F$ ), in correspondence, respectively, with the  $\mathbb{I}$ ,  $\psi$  and  $\sigma$  primary fields. Once combined, because of the  $Z_2$  symmetry of Hamiltonian (24), there are just four independent situations, namely ++, +-, + $F$  and  $FF$ , where the first symbol indicates the boundary condition chosen for the first spin and the second for the last.

For  $FFBC$ , the Hamiltonian can be written in terms of free spinless fermions by means of a Jordan-Wigner transformation [3]. In such case, it can be diagonalized in an exact way, exploiting the properties of free fermions; consequently, the REE's can be computed exactly, following the recipe of Refs. [17, 45]. In the remaining cases, because of the presence of the fixed OBC, the Jordan-Wigner-transformed Hamiltonian is not anymore quadratic at the boundaries, and the use of approximated techniques is a necessity. We perform the computations by means of the density-matrix renormalization group (DMRG) technique [46] in its multi-target version [47]: it allows for a straightforward computation of the REE's of the first excited states of the chain, as well as the implementation of the OBC in an exact way [48]. In any case, we consider systems up to  $L = 1000$  sites; in the DMRG calculations, we employ 7 finite-size sweeps and keep up to 64 states, achieving, in the last steps, a maximum truncation error of the order of  $10^{-8}$ .

What stated in this paragraph also holds for the results of Sections 4 and 5. The obtained numerical data has, in any case, been tested in two independent ways: by comparing the numerical degeneracies of energy multiplets and the ones predicted by CFT (see, e.g., Eq. (31)); by computing the conformal weight of the considered states from the finite-size scaling (FSS) of their energies, according to the CFT formula [33, 34]

$$E_h(L) - E_0(L) = \frac{\pi u}{L} h, \quad (25)$$

being  $E_h(L)$  the energy of the state of weight  $h$  at size  $L$ , and  $u$  the sound velocity of the system, known to be 1 for the spin-1/2 Ising chain in a transverse field and the spin-1/2 XX chain [48]. For the three-state Potts chain, the sound velocity has been extracted numerically from the finite-size scaling of the GS energy density with  $(A, A)$  boundary conditions (see Section 4), i.e., from [33, 34, 48]

$$e_0(L) = e_b + \frac{e_s}{L} + \frac{uc\pi}{24L^2} + o(L^{-2}), \quad (26)$$

where  $e_b$  and  $e_s$  are, respectively, the bulk and surface component of the energy density. For the three-state Potts chain, we obtain  $u = 5/2$  (not shown).

BC	$m$	$h$	$x$	$a_0$	$a_1$	$a_2$	$\eta$	Figure
++	1	2	1/4	0.434	-0.915	0.493	$1.6 \times 10^{-3}$	3(a), (b)
+-	1	3/2	1/2	0.370	0.910	0.487	$3 \times 10^{-3}$	3(c)
+F	1	17/16	1/4	-0.169	-0.965	1.216	$2 \times 10^{-3}$	3(d)
FF	3	2	1/4	0.433	0.921	0.494	$1.4 \times 10^{-3}$	3(e)
FF	2	3/2	1/2	0.872	-0.265	0.444	$1.7 \times 10^{-3}$	3(f)

**Table 1.** Fitting result of the finite-size data for the transverse-field Ising chain with OBC. First column: considered BC; second column: position in the energy spectrum (e.g.,  $m = 1$ : first excited state); third column: conformal weight of the considered state; fourth column: value of  $x$  at which the finite-size fit is performed; fifth, sixth and seventh columns: estimated fit parameters (by means of the formula:  $y = a_0 + a_1 x^{a_2}$ ); eighth column: relative deviation  $\eta$  of  $a_0$  from the CFT prediction; ninth column: corresponding Figure.

To compare our results for model (24) with the CFT predictions we need to identify the low-energy states in the two frameworks. As pointed out by Cardy [43], the operator content of the low-energy effective field theory is affected by the BC in the following way:

$$Z_{++}(q) = \chi_0(q), \quad (27)$$

$$Z_{+-}(q) = \chi_{1/2}(q), \quad (28)$$

$$Z_{+F}(q) = \chi_{1/16}(q), \quad (29)$$

$$Z_{FF}(q) = \chi_0(q) + \chi_{1/2}(q). \quad (30)$$

We can expand these partition functions in powers of  $q$  in order to determine the degeneracies of the excited states [7]:

$$\begin{aligned} q^{c/24} Z_{++}(q) &= 1 + q^2 + \mathcal{O}(q^3), \\ q^{c/24} Z_{+-}(q) &= q^{1/2} + q^{3/2} + \mathcal{O}(q^{5/2}), \\ q^{c/24} Z_{+F}(q) &= q^{1/16} + q^{17/16} + \mathcal{O}(q^{33/16}), \\ q^{c/24} Z_{FF}(q) &= 1 + q^{1/2} + q^{3/2} + q^2 + \mathcal{O}(q^{5/2}). \end{aligned} \quad (31)$$

The first descendant states are, in any case, non degenerate: this makes our task easier, since, in general, the DMRG algorithm, when dealing with degeneracies, considers a non-trivial linear combination in the multiplet. The analysis of such case will be unavoidable when we will study, in Section 5, the spin-1/2 XX chain.

We start the analysis with the ++ case, where the only present tower is the one of the identity. Therefore, the first descendant state is the one associated with the stress-energy tensor, and its  $n = 2$  EEE takes the form in Eq. (20), with  $c = 1/2$ :

$$F_T^{(2)}(x) = \frac{426347 + 53640 \cos(2\pi x) + 38076 \cos(4\pi x) + 6200 \cos(6\pi x) + 25 \cos(8\pi x)}{524288}. \quad (32)$$

We show, in Figure 3(a), the difference between the  $n = 2$  REE for the first excited state and for the GS: as shown in Figure 3(b) and Table 1, a FSS analysis confirms that, in the thermodynamic limit, the DMRG data approaches the CFT prediction with great accuracy. Such non-oscillating (compared to the  $c = 1$  case; see Section 5) finite-size behavior is typical of spin-1/2 XY chains [49, 23], and will be also observed for the three-state Potts chain in Section 4, thus suggesting a general behavior for minimal CFT's.

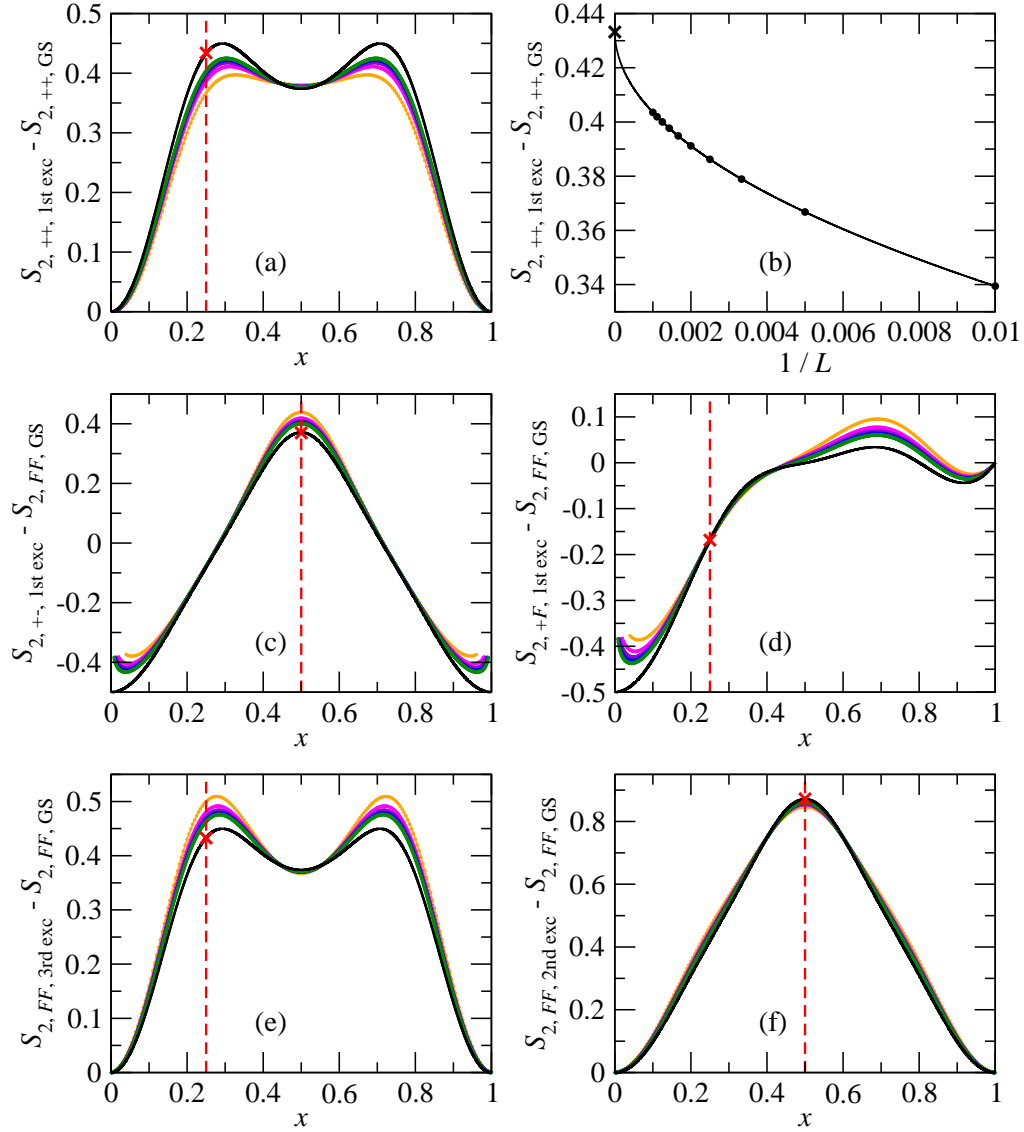


**Figure 3.**  $n = 2$  EEE for the first descendant states of the critical spin-1/2 Ising chain in a transverse field with conformal OBC. Panels (a), (c)-(f): difference between  $S_2$  for the considered descendant state and OBC (see Table 1 for details) and the GS (for some relevant conformal OBC) as a function of  $x$  and for different values of  $L$ . Black line: CFT prediction; colored dotted lines: DMRG data (orange to green:  $L = 200$  to  $1000$ ); vertical red dashed line: considered  $x$  for the FSS analysis (see Table 1 for details); red cross: result of the FSS analysis. Panel (b): FSS of the data of panel (a) at  $x = 1/4$ . Circles: DMRG data; cross: CFT prediction; solid line: best fit, by means of the three-parameters formula  $y = a_0 + a_1 x^{a_2}$  (see Table 1 for the obtained values of the fit parameters and the deviations from the CFT predictions).

We next consider the case of  $+BC$ . The operator content is the tower of the  $\psi$  operator, and the first secondary operator in the tower is  $L_{-1}\psi$ . The relevant four-point function is easily obtained by the Wick theorem [7] ( $\psi$  is a free Fermi field [8]):

$$\langle \psi(z_1)\psi(z_2)\psi(z_3)\psi(z_4) \rangle = \sum_{jklm=1234,1423,2431} \frac{1}{z_{jk}z_{lm}}, \quad (33)$$

Using the relation above and the transformation rule (A.7) we find, with a procedure similar to the one used for the first descendant in the identity tower in Section 2.3,

$$F_{L_{-1}\psi}^{(2)}(x) = \frac{1558 + 439 \cos(2\pi x) + 26 \cos(4\pi x) + 25 \cos(6\pi x)}{2048}. \quad (34)$$

We show in Figure 3(c) the difference between the  $n = 2$  REE for the first excited state and for the GS with  $FFBC$  (for such BC the GS is associated to the identity operator, and therefore taking the difference just the correction due to the secondary operator shall survive, at least apart from finite-size corrections). Also in this case, the agreement between the CFT prediction and the numerical data scaled to the thermodynamic limit is excellent (see table 1 for details). We note that the formalism we have developed is, alone, not able to fully capture the numerical behaviour of the EEE. Indeed, we find that, in order to reproduce it, we have to support Eq. (34) with the additive contribution

$$S_b = \log_2 g, \quad (35)$$

that takes, in the present case, the value  $-1/2$  (i.e.,  $g = 1/\sqrt{2}$ ): it can be interpreted as the Affleck-Ludwig boundary REE [50] associated with the considered BC. The fact that the difference with the entropy of the GS with  $FFBC$  is considered is crucial: indeed, Zhou and collaborators showed, in Ref. [44] and for the GS's, that  $g$  takes the value  $1/\sqrt{2}$  for  $\pm BC$ , and 0 for  $F$ . The same situation, i.e., that the boundary entropy has to be added to the CFT prediction, was observed for primary excited states in Ref. [23].

The third case we consider is the one of  $+FBC$ , leading to a theory containing only the tower of the  $\sigma$  field; the first secondary operator in the theory is thus  $L_{-1}\sigma$ . The four-point function that is relevant for the present case reads [51]:

$$\left\langle \sigma(z_1)^{(+F)} \sigma(z_2)^{(F+)} \sigma(z_3)^{(+F)} \sigma(z_4)^{(F+)} \right\rangle_{\mathbb{C}} = \left( \frac{z_{13}z_{24}}{z_{12}z_{14}z_{23}z_{34}} \right)^{1/8} \sqrt{1 + \sqrt{\frac{z_{12}z_{34}}{z_{13}z_{24}}}}, \quad (36)$$

which is nothing but the conformal block corresponding to the identity channel in the PBC fusion  $\sigma \times \sigma = \mathbb{1} + \epsilon$  [7]. This is the correct four-point function to be considered, since, as argued at the end of Section 2.2, only the fusion channels allowed by the partition function  $Z_{++}$  must be considered (see Eq. (27)). Using Eq. (36) and the transformation rule (A.7) for  $L_{-1}\sigma$ , the  $n = 2$  EEE can be seen to take the form:

$$F_{L_{-1}\sigma}^{(2)} = \frac{1}{512\sqrt{2}} \left( \cos\left(\frac{\pi x}{4}\right) + \sin\left(\frac{\pi x}{4}\right) \right) \left[ -16 \sin\left(\frac{\pi x}{2}\right) + 16 \sin\left(\frac{3\pi x}{2}\right) \right. \\ \left. + 16 \sin\left(\frac{5\pi x}{2}\right) - 16 \sin\left(\frac{7\pi x}{2}\right) - 16 \cos(\pi x) + 60 \cos(2\pi x) + 16 \cos(3\pi x) + 9 \cos(4\pi x) + 443 \right]. \quad (37)$$

Again, we consider, numerically, the first excited state, and we show its  $n = 2$  EEE in Figure 3(d): now, the profile is highly asymmetric with respect to  $x = 1/2$ , because of the different OBC at the boundaries, and interpolates non-trivially between  $-1/2$  and 0. Again a boundary entropy  $-1/2$

has to be added to the CFT prediction in order for it to match the numerical data, and a FSS analysis confirms the correctness of the analytical approach.

The last case we consider is the  $FF$  case, for which the theory contains two characters, relative to the identity and to the  $\psi$  operator. The first descendant states in each tower are, respectively, the third and the second excited states of the chain, corresponding to the stress-energy tensor and to  $L_{-1}\psi$ ; the corrections for them have already been derived and are given by Eqs. (34) and (32). The  $n = 2$  EEE's, obtained using exact diagonalization, are plotted in Figs. 3(e) and (f). In both cases, the agreement between CFT and the FSS-scaled numerical data is remarkable.

To conclude, we were able to interpret the numerical data for the  $n = 2$  EEE's in all the considered situations, finding excellent quantitative agreement with the analytical CFT predictions.

#### 4. $c = 4/5$ minimal CFT and three-state Potts chain

We consider, in this Section, the minimal CFT with central charge  $c = 4/5$  [7]. The operator content of the theory is richer than the one of the  $c = 1/2$  minimal CFT: there are eight primary fields (with respect to an extended  $W$ -algebra), of conformal dimensions 0,  $1/40$ ,  $1/15$ ,  $1/8$ ,  $2/5$ ,  $21/40$ ,  $2/3$  and  $13/8$ .

A lattice realization of the CFT is the three-state Potts chain at its critical point [52]. It is characterized by the Hamiltonian

$$H = -h \sum_j \left( M_j + M_j^\dagger \right) - J \sum_j \left( R_j^\dagger R_{j+1} + R_{j+1}^\dagger R_j \right), \quad (38)$$

where  $j \in \{1, 2, \dots, L\}$  indexes the lattice site, and

$$M_j = \begin{pmatrix} 0 & 1 & 0 \\ 0 & 0 & 1 \\ 1 & 0 & 0 \end{pmatrix}_j, \quad R_j = \begin{pmatrix} e^{i2\pi/3} & 0 & 0 \\ 0 & e^{i4\pi/3} & 0 \\ 0 & 0 & 1 \end{pmatrix}_j. \quad (39)$$

The critical point is at  $h/J = 1$ , realizing the  $c = 4/5$  minimal theory described above. The conformal OBC have been derived by Cardy [37] and by Affleck and collaborators [53]: they are eight, in one-to-one correspondence with the primary fields of the bulk theory. According to the matrix notation used for Hamiltonian (38), the first three of them, that we will call  $A$ ,  $B$  and  $C$ , consist in fixing the boundary state to  $|A\rangle = (1,0,0)^T$ ,  $|B\rangle = (0,1,0)^T$  and  $|C\rangle = (0,0,1)^T$ ; the second three, that we will call  $AB$ ,  $AC$  and  $BC$ , consist in fixing them to  $|AB\rangle = (|A\rangle + |B\rangle)/\sqrt{2}$ ,  $|AC\rangle = (|A\rangle + |C\rangle)/\sqrt{2}$  and  $|BC\rangle = (|B\rangle + |C\rangle)/\sqrt{2}$ ; the  $FBC$  consists in leaving the boundary spin free, and the  $N$  in adding to the Hamiltonian a term, e.g., on the first site, of the form  $-h_1(M_1 + M_1^\dagger)$ , with  $h_1 \ll 0$  [53]. When put together in couples, because of the  $Z_3$  symmetry of Eq. (38), there are fourteen possible choices of conformal OBC:  $(A, A)$ ,  $(A, B)$ ,  $(A, AB)$ ,  $(A, AC)$ ,  $(A, BC)$ ,  $(A, F)$ ,  $(A, N)$ ,  $(AB, AB)$ ,  $(AB, AC)$ ,  $(AB, F)$ ,  $(AB, N)$ ,  $(F, F)$ ,  $(F, N)$  and  $(N, N)$ . We will consider, in the present work, just the three cases  $(A, A)$ ,  $(A, B)$  and  $(A, F)$ .

The corresponding partition functions are given by [37, 53]:

$$Z_{(A,A)}(q) = \chi_0(q), \quad (40)$$

$$Z_{(A,B)}(q) = \chi_{2/3}(q), \quad (41)$$

$$Z_{(A,F)}(q) = \chi_{1/8}(q) + \chi_{13/8}(q). \quad (42)$$

We note that, while in the PBC case the operator content of the three-state Potts chain is reduced to the primary fields of conformal weights 0,  $1/15$ ,  $2/5$  and  $2/3$  [7], by putting on the edges conformal

BC	$h$	$a_0$	$a_1$	$a_2$	$\eta$	Figure
$(A, A)$	0	0.803	-1.458	0.409	$4 \times 10^{-3}$	4(a), (b)
$(A, B)$	2/3	0.870	0.262	0.399	$1.0 \times 10^{-3}$	4(c)
$(A, F)$	1/8	0.222	-0.370	0.431	$3 \times 10^{-3}$	4(d)

**Table 2.** Fitting result of the finite-size data for the GS of the three-state Potts chain with OBC. First column: considered BC; second column: conformal weight of the considered state; third, fourth and fifth columns: estimated fit parameters (used formula:  $y = a_0 + a_1 x^{a_2}$ ); sixth column: relative deviation  $\eta$  of  $a_0$  from the CFT prediction; seventh column: corresponding Figure. The fitted quantity is different in the first and the remaining two cases; see the main text for details about the procedures. In any case, the analysis is performed at a subsystem size  $x = 1/2$ .

OBC as, e.g.,  $(A, F)$ , it is possible to introduce in the model unusual primary fields, occurring in the diagonal theory only [8]. By expanding the partition functions around  $q = 0$ , we obtain:

$$\begin{aligned}
 q^{c/24} Z_{(A,A)}(q) &= 1 + q^2 + \mathcal{O}(q^3), \\
 q^{c/24} Z_{(A,B)}(q) &= q^{2/3} + q^{5/3} + \mathcal{O}(q^2), \\
 q^{c/24} Z_{(A,F)}(q) &= q^{1/8} + q^{9/8} + q^{13/8} + q^{17/8} + q^{21/8} + \mathcal{O}(q^{25/8}).
 \end{aligned}
 \tag{43}$$

In all of the considered cases, the first descendant states are non-degenerate; we will consider, in the towers associated to  $h = 0, 1/8$ , and  $2/3$ , the first descendant states. In addition, we will also consider the  $n = 2$  EEE's of primary states, since their analysis is absent in the literature. The numerical data is obtained by means of the DMRG algorithm, with system sizes up to  $L = 300$ , using up to 7 finite-size sweeps, keeping up to 200 states and achieving a truncation error at the final stages of the finite-system procedure of  $10^{-8}$  or less.

We start by considering the  $(A, A)$  case: the operator content is very simple, since the partition function only contains the character of the identity. The GS is associated with the identity itself, and the  $n$ -th REE's must follow the scaling [13]

$$S_n^{\text{GS}}(x, L) = \frac{c}{12} \left( 1 + \frac{1}{n} \right) \log_2 \left[ \frac{2L}{\pi} \sin(\pi x) \right] + d_1,
 \tag{44}$$

slightly different from Eq. (11), because of the presence of OBC. Such scaling has been verified numerically, by comparing it to the DMRG data, as shown in Figure 4(a): each of the curves in this Figure, corresponding to different values of  $L$ , can be fitted with good precision by means of Eq. (44), but the obtained value of the central charge,  $\gamma(L)$ , suffers from a strong finite-size effect, as shown in Figure 4(b). However, in the same Figure, a simple FSS analysis is performed, in order to show that, in the thermodynamic limit, such values converge to the theoretical one,  $c = 4/5$  (see the caption of Figure 4 for the details of the FSS analysis, and Table 2 for its quantitative results). We were therefore able to show that the  $n = 2$  REE of the GS displays a behavior that is compatible with the scaling (44).

With the same choice of conformal OBC, we consider the first excited state, corresponding to the stress-energy tensor  $T$ . The CFT prediction for the  $n = 2$  EEE, obtained from Eq. (20) by substituting  $c = 4/5$ , looks

$$F_T^{(2)} = \frac{578675 + 196776 \cos(2\pi x) + 36252 \cos(4\pi x) + 7448 \cos(6\pi x) + 49 \cos(8\pi x)}{819200}.
 \tag{45}$$

The comparison with the DMRG data is performed in Figure 5(a): similarly to the case of the GS, the REE suffers from a strong finite-size correction, analogously to the  $c = 1/2$  behavior. With a

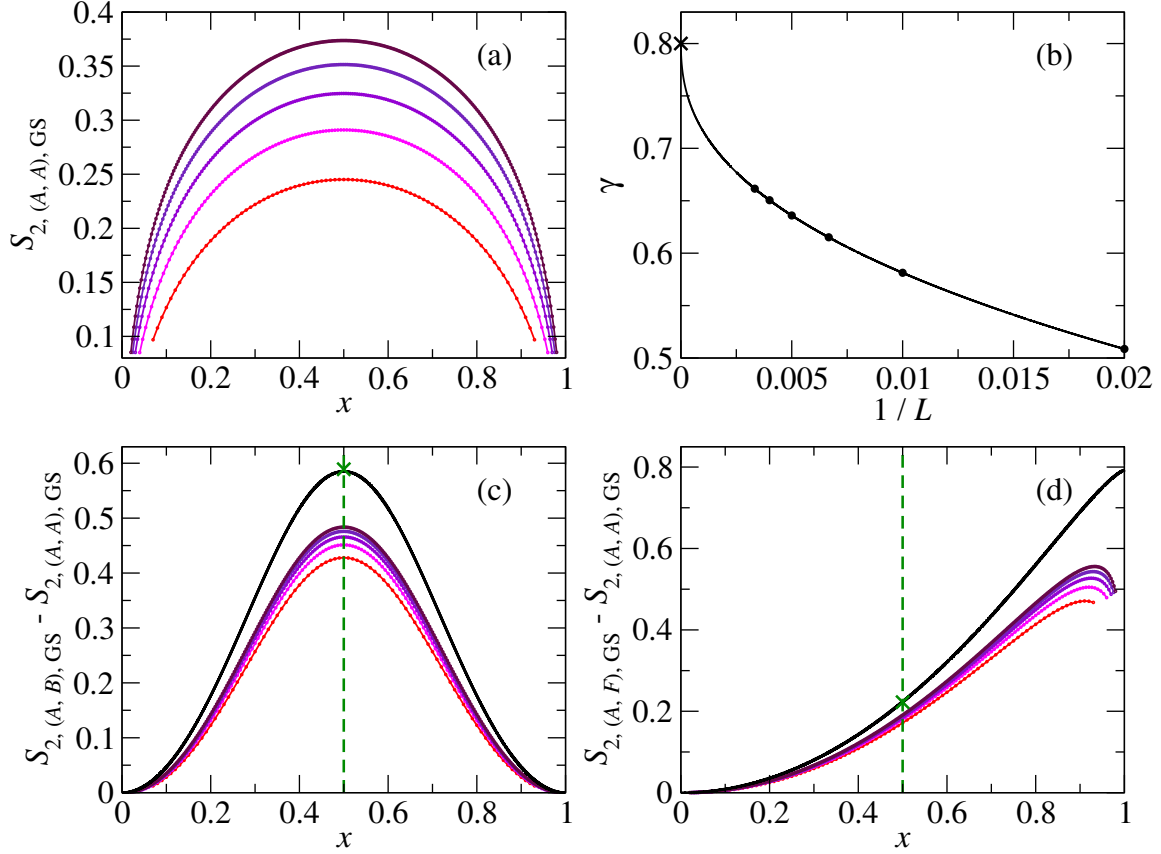


**Figure 4.**  $n = 2$  REE for primary states of the critical three-state Potts chain with conformal OBC. Panel (a):  $S_2$  for the GS with  $(A, A)$ BC at different system sizes. Panels (c) and (d): difference between  $S_2$  for the considered primary state and OBC (see Table 2 for details) and the GS with  $(A, A)$ BC as a function of  $x$  and for different values of  $L$  (see Table 2 for details). Black line: CFT prediction; colored dotted lines: DMRG data (red to maroon:  $L = 100$  to  $300$ ); vertical green dashed line: considered  $x (= 1/2)$  for the FSS analysis; green cross: result of the FSS analysis. Panel (b): FSS of the fitted value of the central charge  $\gamma(L)$ , as obtained from the data in panel (a). Circles: DMRG data; cross: CFT prediction; solid line: best fit, by means of the three-parameters formula  $y = a_0 + a_1 x^{a_2}$  (see Table 2 for the obtained values of the coefficients and the deviations from the CFT predictions).

FSS approach similar to the one of Section 3, we are able to show that the numerical data converges, in the thermodynamic limit, to the CFT prediction: this fact is shown in Figure 5(b) (see Table 3 for quantitative details about the FSS procedure). The agreement between the numerical data and the CFT prediction is remarkable.

We then consider the  $(A, B)$ BC case: the operator content of the theory consists in the tower of the primary field with  $h = 2/3$ , that we dub  $\psi$ . In order to compute the  $n = 2$  EEE we need the four-point function of  $\psi$  operators: we compute it relying on the parafermionic representation of the Potts model [54]. In this representation, the field  $\psi$  is the parafermionic current itself, and its four-point function can be inferred from a recurrence relation. Here, importantly,  $\psi$  is different



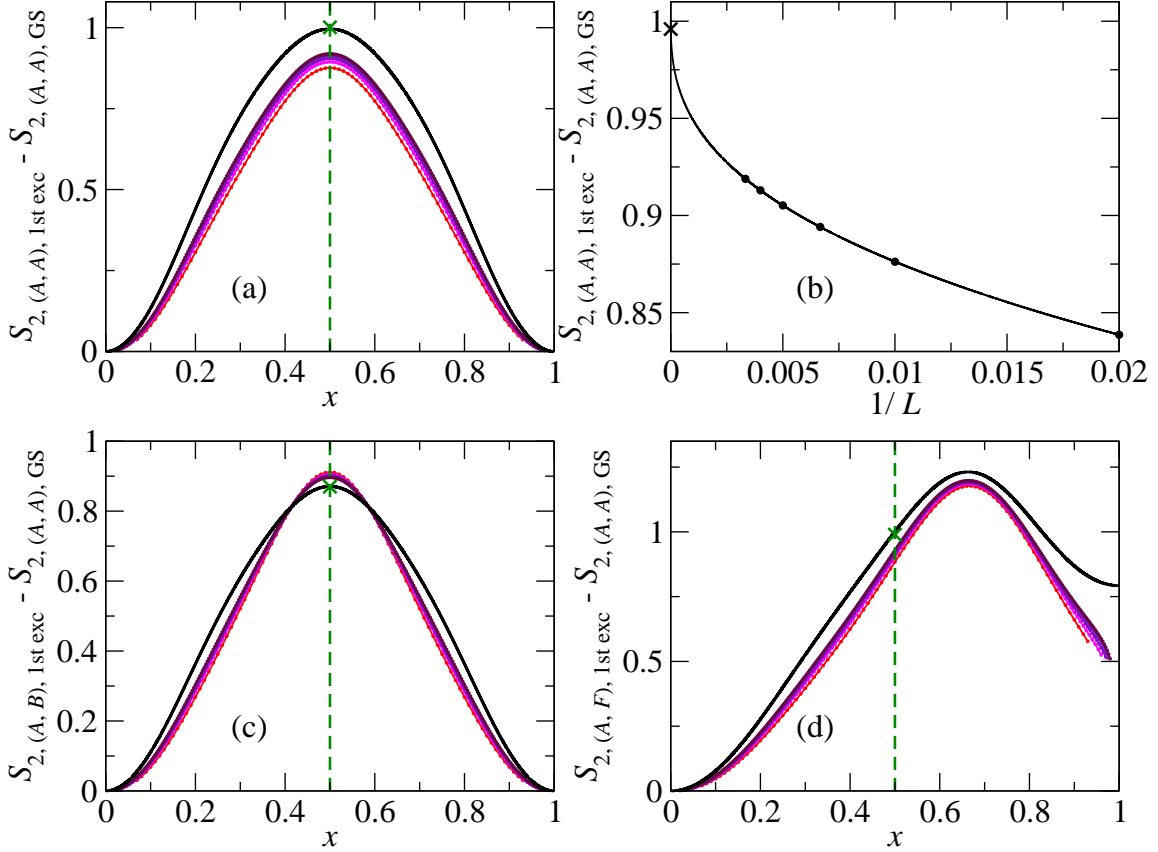


**Figure 5.**  $n = 2$  EEE for descendant states of the critical three-state Potts chain with conformal OBC. Panels (a), (c)-(d): difference between  $S_2$  for the considered descendant state and OBC (see Table 3 for details) and the GS for  $(A, A)BC$ , as a function of  $x$  and for different values of  $L$ . Black line: CFT prediction; colored dotted lines: DMRG data (red to maroon:  $L = 100$  to  $300$ ); vertical green dashed line: considered  $x = 1/2$  for the FSS analysis; green cross: result of the FSS analysis. Panel (b): FSS of the data of panel (a) at  $x = 1/2$ . Circles: DMRG data; cross: CFT prediction; solid line: best fit, done by means of the three-parameters formula  $y = a_0 + a_1 x^{a_2}$  (see Table 3 for the obtained values of the coefficients and the deviations from the CFT predictions).

from its adjoint. The final result reads

$$\langle \psi(z_1) \psi^\dagger(z_2) \psi(z_3) \psi^\dagger(z_4) \rangle = z_{12}^{-1/3} z_{13}^{-2/3} z_{14}^{-1/3} z_{32}^{-1/3} z_{24}^{-2/3} z_{34}^{-1/3} \left[ \frac{z_{14} z_{32}}{z_{12} z_{34}} + \frac{z_{12} z_{34}}{z_{14} z_{32}} - \frac{2}{3} z_{24} \right]. \quad (46)$$

By means of this correlation function, the resulting EEE for the GS is easily computed:

$$F_\psi^{(2)} = \frac{5 + \cos(2\pi x)}{6}. \quad (47)$$

For the first descendant state, applying the technique of Appendix B, we obtain

$$F_{L-1\psi}^{(2)} = \frac{4558 + 1343 \cos(2\pi x) + 194 \cos(4\pi x) + 49 \cos(6\pi x)}{6144}. \quad (48)$$

BC	$h$	$a_0$	$a_1$	$a_2$	$\eta$	Figure
(A, A)	2	1.001	-0.720	0.381	$5 \times 10^{-3}$	5(a), (b)
(A, B)	5/3	0.354	-0.658	0.415	$2 \times 10^{-3}$	5(c)
(A, F)	9/8	0.989	-1.063	0.502	$1.2 \times 10^{-2}$	5(d)

**Table 3.** Fitting result of the finite-size data for the first descendant states of the three-state Potts chain with OBC. First column: considered boundary condition; second column: conformal weight of the considered state; third, fourth and fifth columns: estimated fit parameters (used formula:  $y = a_0 + a_1 x^{a_2}$ ); sixth column: relative deviation  $\eta$  of  $a_0$  from the CFT prediction; seventh column: corresponding Figure. In any case, the analysis is performed at a subsystem size  $x = 1/2$ .

Such predictions are compared with the DMRG data in Figs. 4(c) and 5(c) (for the results of the FSS analysis, see Tables 2 and 3). Again, the agreement between the CFT prediction and the numerical data is remarkable. We point out that in the fusion rule  $\psi \times \psi^\dagger = \mathbb{I}$  only the identity channel is present: accordingly, a different result for the same excited states but with different BC is not possible.

We conclude the Section with the (A, F) case. In order to compute the  $n = 2$  EEE, we need the four-point function of the exotic primary field with scaling dimension  $h = 1/8$ , that we call  $\vartheta$ . This field occupies the (1, 2) position in the Kac table and its four-point function can be calculated by the standard Coulomb-gas approach [7]. For the considered OBC the result is

$$\begin{aligned} \langle \vartheta^{(A,F)}(z_1) \vartheta^{(F,A)}(z_2) \vartheta^{(A,F)}(z_3) \vartheta^{(F,A)}(z_4) \rangle = \\ = z_{12}^{-1/4} z_{13}^{-5/12} z_{14}^{+5/12} z_{23}^{+5/12} z_{24}^{-5/12} z_{34}^{-1/4} {}_2F_1 \left( \frac{1}{6}, \frac{5}{6}; \frac{1}{3}; \frac{z_{12}z_{34}}{z_{13}z_{24}} \right), \end{aligned} \quad (49)$$

where  ${}_2F_1(\alpha, \beta; \gamma; z)$  is the hypergeometric function. The conformal block above corresponds to the identity channel, that is the only one permitted by the fusion rule

$$\vartheta^{(A,F)} \times \vartheta^{(F,A)} = \mathbb{I}^{(A,A)}, \quad (50)$$

which we read off from the partition function  $Z_{A,A}$ , Eq. (40). The EEE for the GS is then

$$F_{\vartheta}^{(2)} = \cos \left( \frac{\pi x}{2} \right)^{\frac{4}{3}} {}_2F_1 \left( \frac{1}{6}, \frac{5}{6}; \frac{1}{3}; y \right), \quad (51)$$

and for the first descendant state we obtain, using Eq. (A.7),

$$\begin{aligned} F_{L^{-1}\vartheta}^{(2)} = \frac{1}{81} \cos \left( \frac{\pi x}{2} \right)^{\frac{4}{3}} \left[ (101 - 156y + 300y^2 - 568y^3 + 324y^4) {}_2F_1 \left( \frac{1}{6}, \frac{5}{6}; \frac{1}{3}; y \right) \right. \\ \left. + (-20 + 44y + 24y^2 - 80y^3 + 24y^4) {}_2F_1 \left( \frac{7}{6}, \frac{5}{6}; \frac{1}{3}; y \right) \right], \end{aligned} \quad (52)$$

with  $y = \sin(\pi x/2)^2$ . We compare the analytical predictions and the DMRG data in Figs. 4(d) and 5(d): after a FSS analysis (see Tables 2 and 3 for quantitative details) we find, again, a nice agreement between them.

Summarizing, we were able to find quantitative agreement between the CFT analytical predictions for the  $n = 2$  EEE's and the DMRG data for all of the considered conformal OBC.

## 5. Compactified free boson and spin-1/2 XX chain

The last CFT we consider is the free boson [7], described by the Lagrangian

$$\mathcal{L} = \frac{1}{8\pi} \int dx [(\partial_t \varphi)^2 - (\partial_x \varphi)^2], \quad (53)$$

compactified on a circle, i.e.,  $\varphi \simeq \varphi + 2\pi R$ ,  $R$  being the compactification radius. This CFT is characterized by a central charge  $c = 1$  and is not minimal; the one-to-one correspondence between primary fields and conformal OBC is therefore not available. Indeed, it is possible to show that the conformal OBC are of two types, named Dirichlet ( $D$ ) and Neumann ( $N$ ) [55].

A simple lattice realization of the compactified free boson is the spin-1/2 XX chain in the vanishing-magnetization (half-filling) sector [2]. In order for it to realize the upper-half-plane CFT, the Hamiltonian to be considered is [56]

$$H = -\frac{J}{2} \sum_j (\sigma_j^+ \sigma_{j+1}^- + \sigma_j^- \sigma_{j+1}^+) - b_1 \sigma_1^x - b_L \sigma_L^x, \quad (54)$$

where  $\sigma_j^\pm = (\sigma_j^x \pm i\sigma_j^y)/2$ ; for  $b_j/J = 0$  ( $b_j/J \gg 0$ ), DBC (NBC) are realized. There are three possible combinations of conformal BC:  $DDBC$ ,  $NNBC$  and  $NDBC$ , respectively associated to the partition functions [55, 56, 23]

$$\begin{aligned} Z_{DD}(q) &= \frac{1}{\eta(q)} \sum_{n \in \mathbb{Z}} q^{n^2/2}, \\ Z_{NN}(q) &= \frac{1}{\eta(q)} \sum_{n \in \mathbb{Z}} q^{2n^2}, \\ Z_{DN}(q) &= \frac{1}{2\eta(q)} \sum_{n \in \mathbb{Z}} q^{(n-1/2)^2/4} = \chi_{1/16}(q) [\chi_0(q) + \chi_{1/2}(q)], \end{aligned} \quad (55)$$

where the last equality, proved in Ref. [23], exploits the naive intuition of additivity of central charges [7]. Once expanded around  $q = 0$ , they look

$$q^{c/24} Z_{DD}(q) = 1 + 2q^{1/2} + q + 2q^{3/2} + 4q^2 + \mathcal{O}(q^{5/2}), \quad (56)$$

$$q^{c/24} Z_{NN}(q) = 1 + q + 4q^2 + 5q^3 + \mathcal{O}(q^4), \quad (57)$$

$$q^{c/24} Z_{DN}(q) = q^{1/16} + q^{9/16} + q^{17/16} + 2q^{25/16} + \mathcal{O}(q^{33/16}). \quad (58)$$

In the theories described by Eqs. (56) and (57), the primary fields are the vertex operators  $:e^{\pm i \frac{n}{R} \varphi}:$ ,  $n \in \mathbb{Z}$  at the compactification radii  $R_{DD} = 1$ ,  $R_{NN} = 1/2$  and the derivative of the field,  $i\partial\varphi$ . The contributions to the REE's originating from them have already been studied in Ref. [23]. In both cases, the first secondary operators have weight 2, and come in multiplets; therefore, the problem of degeneracies cannot be avoided anymore. The case of Eq. (58) has to be treated in a different way, i.e., by opportunely multiplying  $c = 1/2$  corrections, that have already been studied in Ref. [23] and in Section 3.

The numerical data is produced by means of exact diagonalization for  $DDBC$  (in this case, the Hamiltonian can be reduced to a free spinless-fermions one by means of a Jordan-Wigner transformation [2]), and by means of the DMRG technique in the remaining cases. A chain of  $L = 200$  sites has been considered (the FSS analysis for the REE's is unnecessary in this case, for reasons that will be clear soon); 7 finite-size sweeps and up to  $m = 250$  Schmidt states have

been employed; a maximum truncation error of  $10^{-8}$  has been achieved in the last steps of the finite-system algorithm.

We start by considering the case of *DDBC*: as shown by Eq. (56), the excitations at levels  $3/2$  and  $2$  appear in multiplets. First, we consider the fourth and the fifth excited states, corresponding to the operators  $L_{-1}:e^{\pm i\varphi}:$ . The method of Appendix B allows to compute the corresponding  $n = 2$  EEE, starting from the well-known four-point correlations of vertex operators. The final result is

$$F_{L_{-1}:e^{\pm i\varphi}:}^{(2)} = \frac{99 + 28 \cos(2\pi x) + \cos(4\pi x)}{128}, \quad (59)$$

and is plotted, together with the numerical data, in Figure 6(a) (the numerically-computed REE is also the same for both states; however, for linear combinations, it would be different). The agreement between the two approaches is manifest, since the finite-size corrections oscillate as a function of  $x$ . This situation is typical of Luttinger liquids, i.e., free bosonic theories, as proven in many different situations (see, e.g., Refs. [57, 58, 59, 60, 61, 62, 63, 64]).

The sixth, seventh, eighth and ninth excitations are also degenerate, and possess the same conformal weight. However, the first and the second two display different behaviors, as shown in Figs. 6(b) and 6(c). In the CFT picture, there are four operators with conformal dimension 2:  $:e^{\pm i2\varphi}:$ ,  $T$  and  $L_{-1}\partial\varphi$ . In particular, the first two lead to vanishing EEE's [21, 22]. Comparing the prediction for them to the numerical data in Figure 6(b), we see that these two operators identify the sixth and the seventh excitation of the chain. Instead, the profiles of Figure 6(c) are well reproduced by the linear combinations of operators  $T \pm L_{-1}\partial\varphi$ , that lead to the  $n = 2$  EEE

$$F_{T \pm L_{-1}\partial\varphi}^{(2)} = \frac{382659 + 106184 \cos(2\pi x) + 32924 \cos(4\pi x) + 2296 \cos(6\pi x) + 225 \cos(8\pi x)}{524288}. \quad (60)$$

In the case of *NNBC*, the degenerate descendant quadruplet is at level 2, and it is formed by the operators  $T$ ,  $L_{-1}\partial\varphi$  and  $:e^{\pm i\varphi}:$ . The linear combinations of operators that correctly interpret the DMRG data are  $T \pm :\cos\varphi:$  and  $L_{-1}\partial\varphi \pm 2i:\sin\varphi:$ . Remarkably, the first linear combinations correspond to a bosonization of the stress-energy tensor of the  $c = 1/2$  free massless Majorana theory [65]: indeed, we were able to check exactly, by means of the general  $n$ -point function of vertex operators, that such combinations lead to the same functional form, Eq. (32), for the  $n = 2$  EEE as the stress-energy tensor in the  $c = 1/2$  minimal CFT. The CFT prediction is displayed, together with the DMRG data, in Figure 6(d) (the difference between the numerically-computed EEE's for the two states just resides in a relative minus sign in the coefficient of the oscillating part), showing remarkable agreement. Instead, the EEE for the other two states originates from a four-point function involving both  $i\partial\varphi$  and vertex operators. Once explicitly computed, it looks

$$\langle i\partial\varphi(z_1)i\partial\varphi(z_2):e^{i\varphi}(z_3):e^{-i\varphi}(z_4)\rangle = \frac{1}{z_{12}^2 z_{34}^2} + \frac{4}{z_{13}z_{14}z_{23}z_{24}z_{34}^2}, \quad (61)$$

and the resulting EEE's are

$$F_{L_{-1}\partial\varphi \pm 2i:\cos\varphi:}^{(2)} = \frac{[\cos(2\pi x) + 7] [1558 + 439 \cos(2\pi x) + 26 \cos(4\pi x) + 25 \cos(6\pi x)]}{16384}. \quad (62)$$

The successful comparison with the DMRG results is performed in Figure 6(e).

Finally, we consider *DNBC*. This case is different from the previous two, since the partition function can be written as a product of characters of the  $c = 1/2$  minimal CFT [23]. As shown by Eq. (58), the first descendant state arises with a conformal weight  $17/16$ , and stems from the operator  $(L_{-1}\sigma) \otimes \psi$ . The  $n = 2$  EEE is therefore

$$F_{(L_{-1}\sigma) \otimes \psi}^{(2)} = F_{L_{-1}\partial\varphi}^{(2)} F_{\psi}^{(2)}, \quad (63)$$

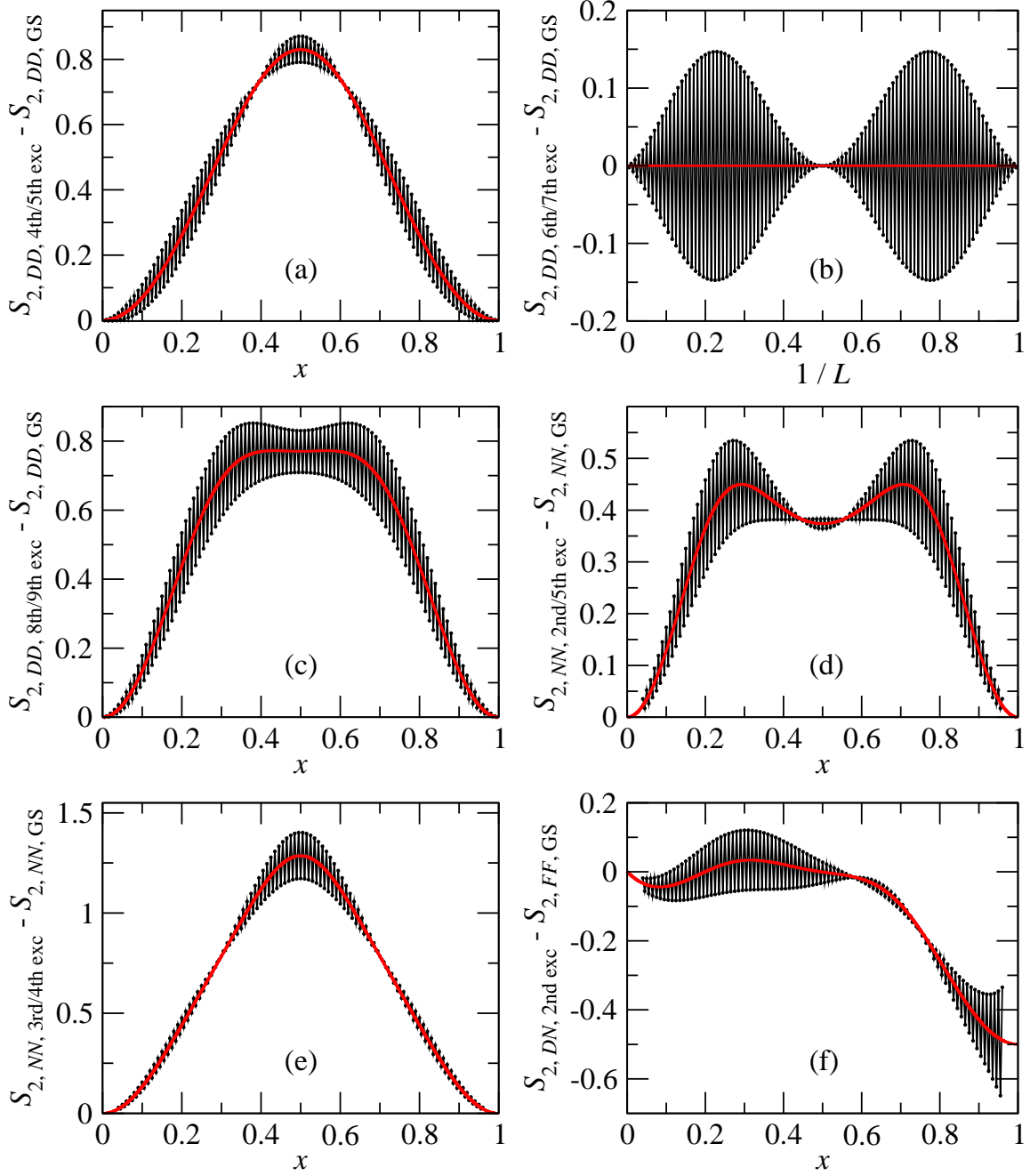


**Figure 6.**  $n = 2$  EEE for descendant excited states of the spin-1/2 XX chain with conformal OBC. Black circles: numerical data; red lines: CFT predictions.

as computed in Section 3 and in Ref. [23]. The comparison with the DMRG data is performed in Figure 6(f): the theoretical prediction and the numerical data match, up to the usual oscillating corrections and to an additive Affleck-Ludwig contribution, with  $g = 1/\sqrt{2}$ , that is known to be associated to NBC [44].

Concluding, even in this case we were able to show that the CFT low-energy picture captures the main features of the numerically computed EEE's.

## 6. Conclusions and outlook

In this work we extended the results of Ref. [24] on Rényi entanglement entropies of descendant states in conformal systems, to the case of conformal systems with boundaries. We provided a unifying approach applicable for both periodic and open boundary conditions and described the computation of the corrections to Eq. (11) for excited states. We also proved that for any choice of boundary conditions the Rényi entanglement entropies are formally given by the same  $2n$ -point functions; the only difference stems from the suppression of one of the chiralities and the different OPE coefficients realized with different boundary conditions (e.g., different conformal blocks solving the same differential equation will play a role with different boundary conditions).

Using this framework we explicitly computed the  $n = 2$  Rényi entanglement entropies for the first few excitation for three lattice models, belonging to different universality classes (Ising, XX or XXZ, and three-state Potts), and compared them with numerical data, obtained by means of the density-matrix-renormalization-group algorithm (and, where available, of free-fermions representations). In all the considered cases, the agreement between analytical predictions and numerical calculations was found to be excellent. Moreover, we were able to solve, for the first time, the problem of the Rényi entanglement entropies of degenerate energy multiplets, where different linear combinations are observed on the lattice and in the field theory.

The study of Rényi entanglement entropies in many-body systems offers several directions for future work. For instance, the understanding of finite-size corrections to the conformal scalings, that we have seen to arise in all of the analyzed situation, although with very different features, is still very incomplete, and deserves further investigation [57, 59, 63]. In addition, the appearance of the Affleck-Ludwig constant contributions as part of the excess Rényi entanglement entropies is a phenomenon that has been observed since many years [44, 23], and its complete theoretical understanding is still lacking. On the other side, Rényi entanglement entropies are among the most natural quantities that can be computed by means of the currently most popular numerical methods [5, 32, 66]. The present study could help in order to numerically identify the lattice realization of conformal boundary conditions: for the majority of critical lattice systems, the boundary conditions preserving conformal invariance are unknown. Moreover, our approach allows, in principle, for the numerical identification of the conformal fields corresponding to specific lattice states, especially for degenerate energy multiplets. We therefore think that our study can stimulate future activity in this fertile research field.

## 7. Acknowledgements

We thank G. Sierra for important discussions, for stimulating our interest in the project and for a careful reading of the manuscript; we thank M. I. Berganza and G. Takács for valuable discussions. We acknowledge INFN-CNAF for providing computational resources and support, and D. Cesini in particular; we thank S. Sinigardi for technical support. L. T. acknowledges financial support from

the EU integrated project SIQS, while T. P. from the Hungarian Academy of Sciences through grant No. LP2012-50 and a postdoctoral fellowship.

### Appendix A. Conformal transformation of generic fields

We review in this Appendix the recipe, introduced in Ref. [36], needed in order to perform the conformal transformation of a generic field. For sake of clarity, only the chiral part of the field is considered.

Primary operators transform in a particularly simple way: the conformal mapping  $w = f(z)$  takes the field  $\Phi$ , with conformal weight  $h$ , to

$$U_f \Phi(z) U_f^{-1} = [f'(z)]^h \Phi(w). \quad (\text{A.1})$$

The transformation rule for secondary fields is much less known, and much more complicated. It is given by

$$U_f \mathcal{O}(z) U_f^{-1} = \sum_{(p)} H_{(p)}[f, z] [L_{p_1} \dots L_{p_k} \mathcal{O}](f(z)), \quad (\text{A.2})$$

where  $L_j$  is the usual  $j$ -th Virasoro generator (relative to the origin), while  $\mathcal{O}(z)$  is the operator corresponding to the state  $\mathcal{O}(0)|0\rangle$ , inserted at  $z$ . The coefficients  $H_{(p)}[f, z]$  were identified, in Ref. [36], to be generated by the expression

$$\begin{aligned} \prod_{n=0}^{\infty} e^{R_n[f, z] L_n} \mathcal{O}(0)|0\rangle &= \left[ \prod_{n=0}^m \sum_{k=0}^{\lfloor \frac{m}{n} \rfloor} \frac{(R_n L_n)^k}{k!} \right] \mathcal{O}(0)|0\rangle \\ &= \sum_{(p)} H_{(p)}[f, z] L_{p_1} \dots L_{p_k} \mathcal{O}(0)|0\rangle, \end{aligned} \quad (\text{A.3})$$

where, in turn, the coefficients  $R_n$  are defined recursively as

$$\begin{aligned} R_0(z) &= \log f'(z), \\ R_n(z) &= \frac{1}{n+1} (R'_{n-1}(z) - A_n(z)), \quad n \geq 1, \end{aligned} \quad (\text{A.4})$$

with  $A_n(z)$  given in Ref. [36], the first few being

$$A_1 = 0, \quad A_2 = R_1^2, \quad A_3 = 0, \quad A_4 = \frac{3}{2} R_2^2, \quad A_5 = 0, \quad A_6 = R_2^3 + 2R_3^2. \quad (\text{A.5})$$

It is easy to check that  $R_2$  is the Schwarzian derivative of  $f$  multiplied by  $1/3!$ , reproducing the familiar transformation law of the stress-energy tensor (Eq. (16)):

$$U_f T(z) U_f^{-1} = [f'(z)]^2 T(f(z)) + \frac{c}{12} \{f, z\}. \quad (\text{A.6})$$

Another example is the transformation law of the field  $\partial\Phi$ , with  $\Phi$  a primary field of weight  $h$ :

$$U_f \partial\Phi(z) U_f^{-1} = [f'(z)]^{h+1} \partial\Phi(f(z)) + h f''(z) [f'(z)]^{h-1} \Phi(f(z)). \quad (\text{A.7})$$

The relation above can independently be deduced from Eq. (A.1) using the chain rule of differentiation.

## Appendix B. Evaluation of $N$ -point functions of descendant fields

We review in this Appendix the strategy, developed in Ref. [24], for evaluating a generic  $N$ -point correlation function of chiral secondary fields.

The basic object that is considered is

$$\langle (L_n A_1)(z_1) A_2(z_2) \dots A_N(z_N) \rangle, \quad (\text{B.1})$$

where  $A_j$  is a generic secondary field, generated from a primary by the application of Virasoro generators. Ultimately, as shown below, such  $N$ -point function can be transformed into a sum of derivatives of the corresponding  $N$ -point function of primary fields.

In the first part of the procedure the generator  $L_n$  is removed from the  $A_1$  operator alone. In order to perform this task, the contour-integral representation of the Virasoro generators is used [7]:

$$L_n \mathcal{O}(z) = \oint_z \frac{d\zeta}{2\pi i} (\zeta - z)^{n+1} T(\zeta) \mathcal{O}(z), \quad (\text{B.2})$$

where the subscript  $z$  indicates that the contour encircles  $z$ . After inserting this expression in Eq. (B.1), the contour of integration can be deformed in order to enclose all the other poles of this integral, i.e., the  $z_j$  insertion points. This gives

$$\begin{aligned} & \left\langle \oint_{z_1} \frac{d\zeta}{2\pi i} (\zeta - z_1)^{n+1} T(\zeta) A_1(z_1) A_2(z_2) \dots A_N(z_N) \right\rangle = \\ & = - \left\langle A_1(z_1) \left[ \oint_{z_2} \frac{d\zeta}{2\pi i} (\zeta - z_1)^{n+1} T(\zeta) A_2(z_2) \right] \dots A_N(z_N) \right\rangle - \\ & \quad - \left\langle A_1(z_1) A_2(z_2) \left[ \oint_{z_3} \frac{d\zeta}{2\pi i} (\zeta - z_1)^{n+1} T(\zeta) A_3(z_3) \right] \dots A_N(z_N) \right\rangle - \dots \end{aligned} \quad (\text{B.3})$$

Now, using the relation

$$(\zeta - z_1)^{n+1} = \sum_{k=0}^{\infty} \binom{n+1}{k} (z_i - z_1)^{n+1-k} (\zeta - z_i)^k, \quad (\text{B.4})$$

and so on, the integrals can be removed and replaced by Virasoro generators acting on the operators  $A_{j>1}$ :

$$\begin{aligned} & \langle (L_n A_1)(z_1) A_2(z_2) \dots A_N(z_N) \rangle = \\ & = - \sum_{k=-1}^{\infty} \binom{n+1}{k+1} (z_2 - z_1)^{n-k} \langle A_1(z_1) (L_k A_2)(z_2) \dots A_N(z_N) \rangle - \\ & \quad - \sum_{k=-1}^{\infty} \binom{n+1}{k+1} (z_3 - z_1)^{n-k} \langle A_1(z_1) A_2(z_2) (L_k A_3)(z_3) \dots A_N(z_N) \rangle - \dots \end{aligned} \quad (\text{B.5})$$

Iterating this procedure, all the Virasoro generators can be removed from  $A_1$ , paying the price of complicating the remaining operators in the correlator: indeed, what is obtained is a finite sum of correlators, with the operator inserted at  $z_1$  being primary.

The next step consists in repeating the procedure above for  $A_2$ , reducing it to a primary. However, at this point, Virasoro generators with  $n = -1, 0$  will appear again in front of the first



operator, potentially followed by other Virasoro generator of any order: this apparently could make all the previous efforts useless. Actually, this is not the case, because of the following identity:

$$L_n L_{-1}^m \Phi = c_{nm} L_{-1}^{m-n} \Phi, \quad n \geq -1;$$

$\Phi$  is a primary field, indicating that the addition of Virasoro generators in front of powers of  $L_{-1}$  results in a sequence of  $L_{-1}$  generators, i.e., a partial derivative. The final result is then

$$\sum_j C_j(z_1, \dots, z_N) \partial_{z_1}^{m_{1j}} \partial_{z_2}^{m_{2j}} \dots \partial_{z_{N-1}}^{m_{N-1,j}} \langle \Phi_1(z_1) \Phi_2(z_2) \dots \Phi_N(z_N) \rangle, \quad (\text{B.6})$$

with proper  $C_j(z_1, \dots, z_N)$  coefficients and  $\Phi_j$  all primaries. Therefore, everything is reduced to the computation of sums of derivatives of  $N$ -point functions of primaries, computable by means of, e.g., the Coulomb gas formalism [7] in the case of minimal models.

## References

- [1] L. Amico, R. Fazio, A. Osterloh, and V. Vedral, *Rev. Mod. Phys.* **80**, 517 (2008).
- [2] T. Giamarchi, *Quantum Physics in One Dimension* (Oxford University Press, Oxford, 2003).
- [3] S. Sachdev, *Quantum Phase Transitions* (Cambridge University Press, Cambridge, 2011).
- [4] M. Takahashi, *Thermodynamics of One-Dimensional Solvable Models* (Cambridge University Press, Cambridge, 1999).
- [5] U. Schollwöck, *Ann. Phys.* **326**, 96 (2011).
- [6] M. Henkel, *Conformal Invariance and Critical Phenomena* (Springer, Berlin, 1999).
- [7] P. Di Francesco, P. Mathieu, and D. Sénéchal, *Conformal Field Theory* (Springer-Verlag, New York, 1997).
- [8] G. Mussardo, *Statistical Field Theory* (Oxford University Press, Oxford, 2010).
- [9] A. A. Belavin, A. M. Polyakov, and A. B. Zamolodchikov, *Nucl. Phys. B* **241**, 333 (1984).
- [10] A. Rényi, *Probability Theory* (Dover, Mineola, 2007).
- [11] M. A. Nielsen and I. L. Chuang, *Quantum Computation and Quantum Information* (Cambridge University Press, Cambridge, 2000).
- [12] C. Holzhey, F. Larsen, and F. Wilczek, *Nucl. Phys. B* **424**, 443 (1994).
- [13] P. Calabrese and J. Cardy, *J. Stat. Mech.* P06002 (2004).
- [14] J. Eisert, M. Cramer, and M. B. Plenio, *Rev. Mod. Phys.* **82**, 277 (2010).
- [15] M. B. Hastings, *J. Stat. Mech.* P08024 (2007).
- [16] Y. Huang, arXiv:1403.0327.
- [17] G. Vidal, J. I. Latorre, E. Rico, and A. Kitaev, *Phys. Rev. Lett.* **90**, 227902 (2003).
- [18] S. Barbarino, L. Taddia, D. Rossini, L. Mazza, and R. Fazio, *Nat. Comm.* **6**, 8134 (2015).
- [19] R. Islam, R. Ma, P. M. Preiss, M. E. Tai, A. Lukin, M. Rispoli, and M. Greiner, arXiv:1509.01160.
- [20] A. M. Kaufman, M. E. Tai, A. Lukin, M. Rispoli, R. Schittko, P. M. Preiss, and M. Greiner, arXiv:1603.04409.
- [21] F. C. Alcaraz, M. I. Berganza, and G. Sierra, *Phys. Rev. Lett.* **106**, 201601 (2011).
- [22] M. I. Berganza, F. C. Alcaraz, and G. Sierra, *J. Stat. Mech.* P01016 (2012).
- [23] L. Taddia, J. C. Xavier, F. C. Alcaraz, and G. Sierra, *Phys. Rev. B* **88**, 075112 (2013).
- [24] T. Palmai, *Phys. Rev. B* **90**, 161404(R) (2014).
- [25] P. Caputa and A. Veliz-Osorio, *Phys. Rev. D* **92**, 065010 (2015).
- [26] B. Chen, W. Guo, S. He, and J. Wu, *JHEP* **15**, 173 (2015).
- [27] I. Affleck, *Conformal Field Theory Approach to Quantum Impurity Problems* in G. Morandi, P. Sodano, A. Tagliacozzo, and V. Tognetti (eds.), *Field Theories for Low-Dimensional Condensed Matter Systems* (Springer, Berlin, 2000).
- [28] J. Polchinski, *String Theory* (Cambridge University Press, Cambridge, 1998).
- [29] D. Bianchini, O. Castro-Alvaredo, B. Doyon, E. Levi, and F. Ravanini, *J. Phys. A: Math. Theor.* **48**, 04FT01 (2015).
- [30] J. L. Cardy, O. Castro-Alvaredo, and B. Doyon, *J. Stat. Phys.* **130**, 7451 (2007)
- [31] G. Sárosi and T. Ugajin, arXiv:1603.03057.
- [32] S. Humeniuk and T. Roscilde, *Phys. Rev. B* **86**, 235116 (2012).
- [33] H. W. J. Blöte, J. L. Cardy, and M. P. Nightingale, *Phys. Rev. Lett.* **56**, 742 (1986).
- [34] I. Affleck, *Phys. Rev. Lett.* **56**, 746 (1986).
- [35] M. R. Gaberdiel, *Rep. Prog. Phys.* **63** 607 (2000).

- [36] M. Gaberdiel, Phys. Lett. B **325**, 366 (1994).
- [37] J. L. Cardy, Nucl. Phys. B **324**, 581 (1989).
- [38] I. Runkel, Nucl. Phys. B **549**, 563 (1999).
- [39] I. Runkel, Nucl. Phys. B **579**, 561 (2000).
- [40] J. F. Gomes, Phys. Lett. B **171**, 75 (1986).
- [41] T. Nishioka, S. Ryu, and T. Takayanagi, J. Phys. A: Math. Theor. **42**, 504008 (2009).
- [42] J. Bhattacharya, M. Nozaki, T. Takayanagi, T. Ugajin, Phys. Rev. Lett. **110**, 091602 (2013).
- [43] J. L. Cardy, Nucl. Phys. B **275**, 200 (1986).
- [44] H. Q. Zhou, T. Barthel, J. O. Fjærestad, and U. Schollwöck, Phys. Rev. A **74**, 050305(R) (2006).
- [45] I. Peschel, J. Phys. A: Math. Gen. **36**, L205 (2003).
- [46] S. R. White, Phys. Rev. Lett. **69**, 2863 (1992).
- [47] C. Degli Esposti Boschi and F. Ortolani, Eur. Phys. J. B **41**, 503 (2004).
- [48] L. Taddia, *Entanglement Entropies in One-Dimensional Systems* (Lambert Academic Publishing, Saarbrücken, 2014).
- [49] F. Iglói and R. Juhász, Europhys. Lett. **81**, 57003 (2008).
- [50] I. Affleck and A. W. W. Ludwig, Phys. Rev. Lett. **67**, 161 (1991).
- [51] E. Ardonne and G. Sierra, J. Phys. A: Math. Theor. **43**, 505402 (2010).
- [52] F. Y. Wu, Rev. Mod. Phys. **54**, 235 (1982).
- [53] I. Affleck, M. Oshikawa, and H. Saleur, J. Phys. A: Math. Gen. **31**, 5827 (1998).
- [54] A. B. Zamolodchikov and V. A. Fateev, Sov. Phys. JETP **62**, 215 (1985).
- [55] H. Saleur, arXiv:cond-mat/9812110.
- [56] U. Bilstein, J. Phys. A: Math. Gen. **33**, 4437 (2000).
- [57] N. Laflorencie, E. S. Sørensen, M.-S. Chang, and I. Affleck, Phys. Rev. Lett. **96**, 100603 (2006).
- [58] J. Cardy and P. Calabrese, J. Stat. Mech. P04023 (2010).
- [59] P. Calabrese, M. Campostrini, F. Essler, and B. Nienhuis, Phys. Rev. Lett. **104** 095701 (2010).
- [60] M. Dalmonte, E. Ercolessi, and L. Taddia, Phys. Rev. B **84**, 085110 (2011).
- [61] J. C. Xavier and F. C. Alcaraz, Phys. Rev. B **85**, 024418 (2012).
- [62] M. Dalmonte, E. Ercolessi, and L. Taddia, Phys. Rev. B **85**, 165112 (2012).
- [63] B. Swingle, J. McMinis, and N. M. Tubman, Phys. Rev. B **87**, 235112 (2013).
- [64] L. Cevolani, arXiv:1601.01709.
- [65] E. B. Kiritsis, Phys. Lett. B **198**, 379 (1987).
- [66] W. J. Porter and J. E. Drut, arXiv:1605.07085.